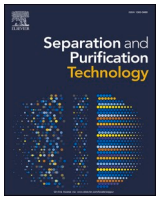
Separation and Purification Technology 336 (2024) 126275



Contents lists available at ScienceDirect

Separation and Purification Technology

journal homepage: www.elsevier.com/locate/seppur



Dry particle size separation using electrostatic traveling wave methods

Yue Yu [a,b], Jan Cilliers [a,b,*], Kathryn Hadler [b,c], Stanley Starr [b], Yanghua Wang [a,b,*]

[a] Resource Geophysics Academy, Imperial College London, London SW7 2BP, UK
[b] Department of Earth Science and Engineering, Imperial College London, London SW7 2AZ, UK
[c] European Space Resources Innovation Centre (ESRIC), L-4362 Esch-sur-Alzette, Luxembourg

ARTICLE INFO

Editor: Luo Guangsheng

Keywords:
Dielectrophoresis
Electrostatic travelling wave
Field frequency
Particle transport
Particle separation
Particle size

ABSTRACT

Electrostatic traveling wave (ETW) methods have grown in popularity as a method to manipulate and separate fine particles. This is of interest to mineral processing and In-situ Space Resource Utilization. Here, we demonstrate that ETW can be used to separate particles by size. First, our numerical calculation and simulation results show the competing effect of DEP and Coulomb force on particle motion direction, which depends on the frequency, particle size and charge. Then we define the "crossover frequency" allowing prediction of operating parameters to separate particles. At the "crossover frequency" – a particle is equally likely to move forward or backward. The crossover frequency decreases as particle size increases, and the proportion of particles moving backward increases as frequency increases. Four size groups of ballotini particles (glass) were transported and collected at different wave field frequencies. Finally, we have demonstrated experimentally the separation of particles between 30–50 μm and 75–110 μm. Simulation and experiment results revealed the effects of frequency, particle size and charge on particle motions. And the model can be used to guide the design of separation systems.

1. Introduction

1.1. Dry particle separation

Reducing water usage in mineral processing is beneficial for global environmental protection [1,2]. Also, the cost of water resources in remote mining areas and locations like Australia and Chile is increasing [3,4]. In the space environment, many essential technological methods, such as dust mitigation for spacecrafts, beneficiation process in the In-situ Space Resource Utilization (ISRU), water treatment is not applicable [5]. In addition, in the processing of particles when conducting research, dry particle manipulation is crucial [6,7]. Therefore, the development of dry particle processing is in great demand.

1.2. Introduction, development and merits of ETW methods

Electrostatic traveling wave (ETW) methods have received increased attention for dry particle transport and separation [8]. ETW systems control the motion of particles by manipulating Coulomb and dielectrophoresis forces. These forces are due to the particles' physical properties, as well as the ETW field characteristics, which can be tailored by the design of system parameters, such as applied voltage and electrode configurations. The ETW methods have the advantages of a simple structure, lack of moving parts, and high applicability for different types of particles.

The earliest concept of ETW, the method of 'electric curtain' was first applied by Masuda and coworkers in the connection with charged aerosol clouds transportation [9–11]. They also conducted experiments and developed simulation models on the movement of blood cell and separation of particles in liquids [12,13]. In their theory, the wave field was simplified to the combination of two harmonic waves propagating in different directions. And if particles with different properties carried by different waves and move in different directions, the transport and separation of particles could be achieved simultaneously.

Subsequently, more efforts were made to understand the experiment phenomenon quantitatively and to design improved devices [14–16]. Machowski and coworkers [17] performed the separation experiments on sand and pulverised alumina powders by testing different shapes of electrodes, such as cylinder and stripe. They found sand was transported along the traveling wave while alumina was transported oppositely at

* Department of Earth Science and Engineering, Imperial College London, London SW7 2AZ, UK (J. Cilliers). Resource Geophysics Academy, Imperial College London, London SW7 2BP, UK (Y. Wang).
E-mail addresses: j.j.cilliers@imperial.ac.uk (J. Cilliers), yanghua.wang@imperial.ac.uk (Y. Wang).

https://doi.org/10.1016/j.seppur.2024.126275
Received 27 October 2023; Received in revised form 21 December 2023; Accepted 1 January 2024
Available online 2 January 2024
1383-5866/Crown Copyright © 2024 Published by Elsevier B.V. This is an open access article under the CC BY license (http://creativecommons.org/licenses/by/4.0/).

lower frequencies. And at higher frequencies, both the motion directions of sand and alumina reversed due to the transition of motion mode.

Recent advances have been made in developing theories of particle motion for ETW methods [18–20]. Kawamoto and coworkers [21] adopted a 3-D modified hard-sphere DEM model to predict the particle motion in the lunar environment. By adjusting the balance of the gravitation force and Coulomb force on different sizes of particles, the particles smaller than 20 μm significantly flew higher above the conveyor board and could be separated in a vacuum chamber. Zouaghi and coworkers [22–25] have also made systematic investigations on the particle motion mechanisms, especially on the explanation of backward motion. They have revealed the important effect of particle size and operating frequency.

The research on the design of dust mitigation and the toner transport technologies using ETW methods have advanced much more than that of particle separation [26–32]. This is because dust mitigation or toner transport does not require the strict control of particle trajectories as does particle separation. Particle separation systems design must precisely consider the relevant properties of the particles to be separated. Currently particle separation systems are poorly understood because the underlying theory of particle motion is poorly understood.

1.3. Summary of work

In this paper, the principles for the separation are analysed including the effects of dielectrophoresis on large particles and a comparison of the effects of the Coulomb and DEP forces.

We developed an ETW experimental system to study particle transportation. Four distinct particle size groups were used. The particles were transported either forward or backward and collected in bins at the ends of the apparatus. We measured the collected mass in both forward and backward directions plus the particles remaining on the array. Each of these particle cohorts were analysed by size. The fraction of particles transported in each direction exhibited a noticeable frequency-dependent effect. At lower frequencies, a majority of particles moved forward, but as the frequency increased, the fraction of particles being transported backward increased.

We plotted two lines indicating the mass fraction of particles of each size range cohort collected in forward and backward directions related to frequency. These plots exhibited a crossover point. The frequency corresponding this point is defined as “crossover” frequency, which means a particle has an equal chance to move forward or backward. And the crossover frequency decreases as the particle size increases.

The experimental results show that larger particles tend to move backward at lower frequencies, at which frequency smaller particles may still move forward effectively. Using the single size transporting data, we could estimate the size concentration of a mixture of different sizes of particles in forward and backward directions. And the separation performance of particles of various sizes at different frequencies are predicted.

Finally, a mixture of different sizes of 30–50 μm and 75–110 μm particles have been tested and show good separation performance. And the mass recovery of each size of particle in forward and backward directions match well with the estimation of the mass recovery using the single size particle transport experiment results.

2. Principles of separation

2.1. Particle motion direction

The formula for a nonuniform electrostatic traveling field can be expressed as a Fourier series. The higher order terms of Fourier series decay fast so only the first and second terms are of importance and considered. In a 2-D model, the electric field generated by three-phase sinusoidal waves in the horizontal and vertical directions can be found [33]:

$$\begin{cases} E_x = V_A\left(\dfrac{3a_1\alpha_1}{2}\sin(\alpha_1 x-\omega t)\exp(-\alpha_1 y)+\dfrac{3a_2\alpha_2}{2}\sin(\alpha_2 x+\omega t)\exp(-\alpha_2 y)\right) \\ E_y = V_A\left(\dfrac{3a_1\alpha_1}{2}\cos(\alpha_1 x-\omega t)\exp(-\alpha_1 y)+\dfrac{3a_2\alpha_2}{2}\cos(\alpha_2 x+\omega t)\exp(-\alpha_2 y)\right) \end{cases} \tag{1}$$

where V_A is the amplitude of applied voltage, a_1 and a_2 are coefficients dependent on the electrode configuration, $\alpha_n = 2n\pi/\lambda$, λ is the wavelength, ω is the angular frequency, x and y represent the positions on the horizontal and vertical axes of the Cartesian coordinate system. The wave velocity of the first and second wave is ω/α_1 and $-\omega/\alpha_2$, respectively.

The traveling direction of electrostatic wave field is consistent with the dominate first term wave direction. Under the pure perfect single wave, particle will move along the wave in the same direction.

2.2. Effect of harmonic wave

The effects of backward harmonic wave on the particle backward motion have been explained in the literature [12,22,34,35]. Note that our prior work demonstrated that the addition factors of lower levitation height and higher frequency increase the probability of a particle moving backward due to the action of the harmonic wave [33]. The actual motion direction of particles is determined by the interaction of two waves. Thus, if the parameters of the field such as frequency and amplitude are adjusted to allow one type of particle to interact with one of the wave streams and the rest with the other, the separation and the transport of the particle can be achieved simultaneously.

2.3. Effect of dielectrophoresis

The term “dielectrophoresis” (DEP) was coined by H. A. Pohl [36] in the research of precipitation suspensoids in fluids. In our case, the effect of dielectrophoresis becomes important for relatively large particles with low charge.

According to the theory of calculating DEP [37], the dipole moment of a particle in the field is calculated as:

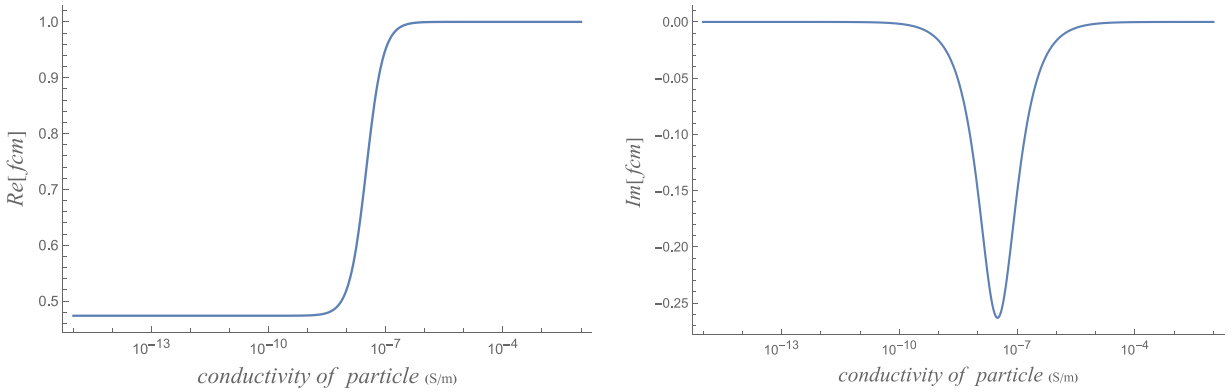
$$\boldsymbol{m} = m_x(t)\boldsymbol{a_x} + m_y(t)\boldsymbol{a_y} \tag{2}$$

where:

$$\begin{aligned} m_x(t) &= -4\pi\varepsilon_m r^3\frac{3a_1\alpha_1}{2}\exp(-\alpha_1 y)|f_{CM}|\sin(\omega t-\alpha_1 x-\varphi_m) \\ &\quad +4\pi\varepsilon_m r^3\frac{3a_2\alpha_2}{2}\exp(-\alpha_2 y)|f_{CM}|\sin(\omega t+\alpha_2 x-\varphi_m) \\ &= -4\pi\varepsilon_m r^3\frac{3a_1\alpha_1}{2}\exp(-\alpha_1 y)\{\mathrm{Re}[f_{CM}]\sin(\omega t-\alpha_1 x)+\mathrm{Im}[f_{CM}]\cos(\omega t-\alpha_1 x)\} \\ &\quad +4\pi\varepsilon_m r^3\frac{3a_2\alpha_2}{2}\exp(-\alpha_2 y)\{\mathrm{Re}[f_{CM}]\sin(\omega t+\alpha_2 x)+\mathrm{Im}[f_{CM}]\cos(\omega t+\alpha_2 x)\} \end{aligned} \tag{3}$$

$$\begin{aligned} m_y(t) &= 4\pi\varepsilon_m r^3\frac{3a_1\alpha_1}{2}\exp(-\alpha_1 y)|f_{CM}|\cos(\omega t-\alpha_1 x-\varphi_m) \\ &\quad +4\pi\varepsilon_m r^3\frac{3a_2\alpha_2}{2}\exp(-\alpha_2 y)|f_{CM}|\cos(\omega t+\alpha_2 x-\varphi_m) \\ &= 4\pi\varepsilon_m r^3\frac{3a_1\alpha_1}{2}\exp(-\alpha_1 y)\{\mathrm{Re}[f_{CM}]\cos(\omega t-\alpha_1 x)-\mathrm{Im}[f_{CM}]\sin(\omega t-\alpha_1 x)\} \\ &\quad +4\pi\varepsilon_m r^3\frac{3a_2\alpha_2}{2}\exp(-\alpha_2 y)\{\mathrm{Re}[f_{CM}]\cos(\omega t+\alpha_2 x)-\mathrm{Im}[f_{CM}]\sin(\omega t+\alpha_2 x)\} \end{aligned} \tag{4}$$

where ε_m is the relative dielectric permittivity, r is the particle radius, and f_{CM} is the Clausius-Mossotti factor:



(a) Real part value of f_{CM} (b) Imaginary part value of f_{CM}

Fig. 1. DEP in the x direction.

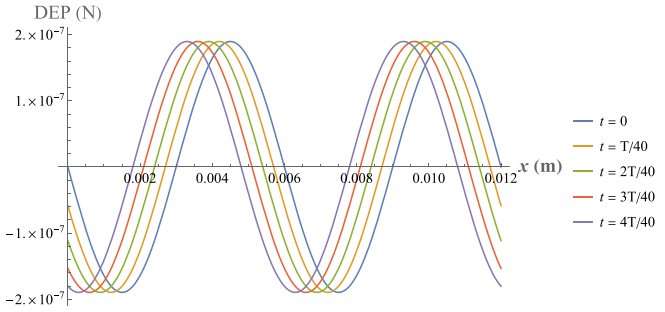


Fig. 2. DEP in the x direction for a 0.2 mm glass particle size.

$$f_{CM} = \frac{\varepsilon_p^*(\omega) - \varepsilon_m^*(\omega)}{\varepsilon_p^*(\omega) + 2\varepsilon_m^*(\omega)} \tag{5}$$

where ε_p^* and ε_m^* are the complex dielectric permittivity of particle and medium, which are related to angular frequency (ω) of the electric field. The complex permittivity is given as:

$$\varepsilon^* = \varepsilon - i\sigma/\omega \tag{6}$$

where σ is the conductivity, and $i^2 = -1$.

The time-dependent DEP is calculated as:

$$\boldsymbol{F}(t) = F_x(t)\boldsymbol{a_x} + F_y(t)\boldsymbol{a_y} \tag{7}$$

where:

$$F_x(t) = m_x(t)\frac{\partial E_x(t)}{\partial x} + m_y(t)\frac{\partial E_x(t)}{\partial y} \tag{8}$$

and

$$F_y(t) = m_x(t)\frac{\partial E_x(t)}{\partial y} + m_y(t)\frac{\partial E_y(t)}{\partial y} \tag{9}$$

The time-dependent DEP in the x direction is simplified in the form associated with real part Re[f_{CM}] and imaginary part Im[f_{CM}], respectively:

$$\begin{aligned} F_x(t) &= m_x(t)\frac{\partial E_x(t)}{\partial x} + m_y(t)\frac{\partial E_x(t)}{\partial y} \\ &= -18\pi\varepsilon_m r^3 \mathrm{Re}[f_{CM}]a_1a_2\alpha_1^3\exp(-3\alpha_1 y)\sin(\alpha_1 x + 2\omega t) \\ &-9\pi\varepsilon_m r^3 \mathrm{Im}[f_{CM}]\alpha_1^3\exp(-4\alpha_1 y)\{8a_2^2 + a_1\exp(\alpha_1 y)[4a_2\cos(3\alpha_1 x) + 2a_2\cos(2\alpha_1 x - 2\omega t) + a_1\exp(\alpha_1 y)\cos(2\alpha_1 x - 2\omega t)]\} \end{aligned} \tag{10}$$

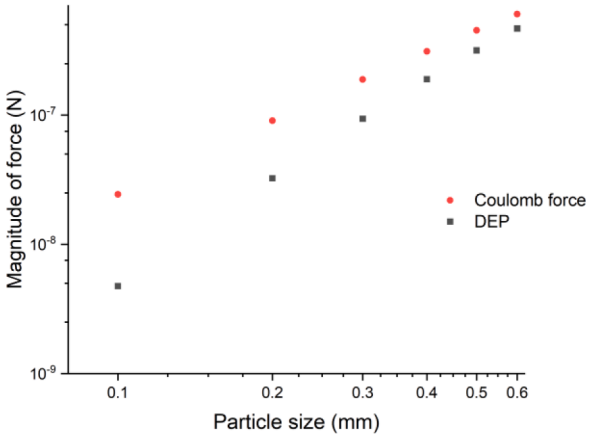


Fig. 3. Comparison of maximum force on particle.

The ETW field generates both traveling DEP and standing DEP, which are associated with Im[f_{CM}] and Re[f f_{CM}], respectively. It usually defines the phase-dependent portion of the field as traveling DEP. The relationship between the value of Re[f_{CM}] and Im[f_{CM}] at the frequency of 100 Hz, and conductivity of a particle in air is shown in Fig. 1. Because the conductivity of the glass is smaller than 10^{-13}, the Im[f_{CM}] is much smaller than Re[f_{CM}] for a glass particle in air. Only the component of DEP associated with the real part of Clausius-Mossotti factor is considered.

The wave velocity of the standing DEP is $-2\alpha_1/\omega$. The negative velocity means the DEP is directed backward, which definitely contributes to the backward motion of particles. The traveling direction of DEP can also be found from the plots of DEP on the 0.2 mm glass particle in the x direction at a height of $y = 0.2$ mm at different time in a period of T (0.02 s) in Fig. 2.

Assuming a particle with a charge of 1 % of the saturation charge is at any positions on the board, Fig. 3 compares the peak value of DEP and Coulomb forces acting on it with various sizes. The saturation charge is calculated by the relation of Pauthenier [38], which is directly

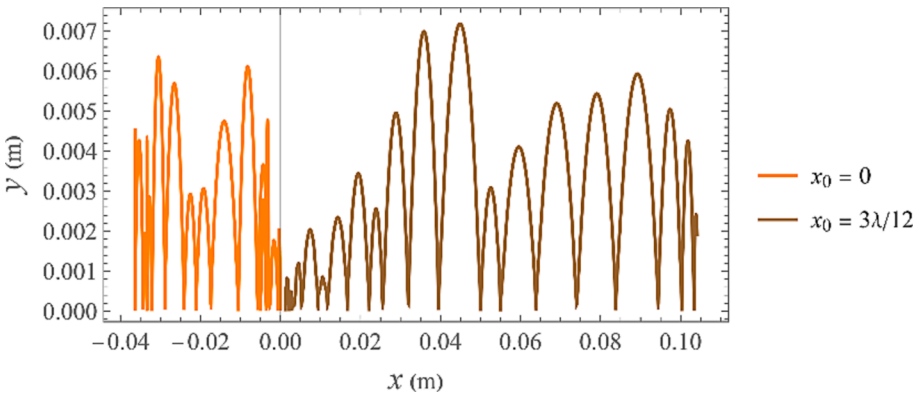
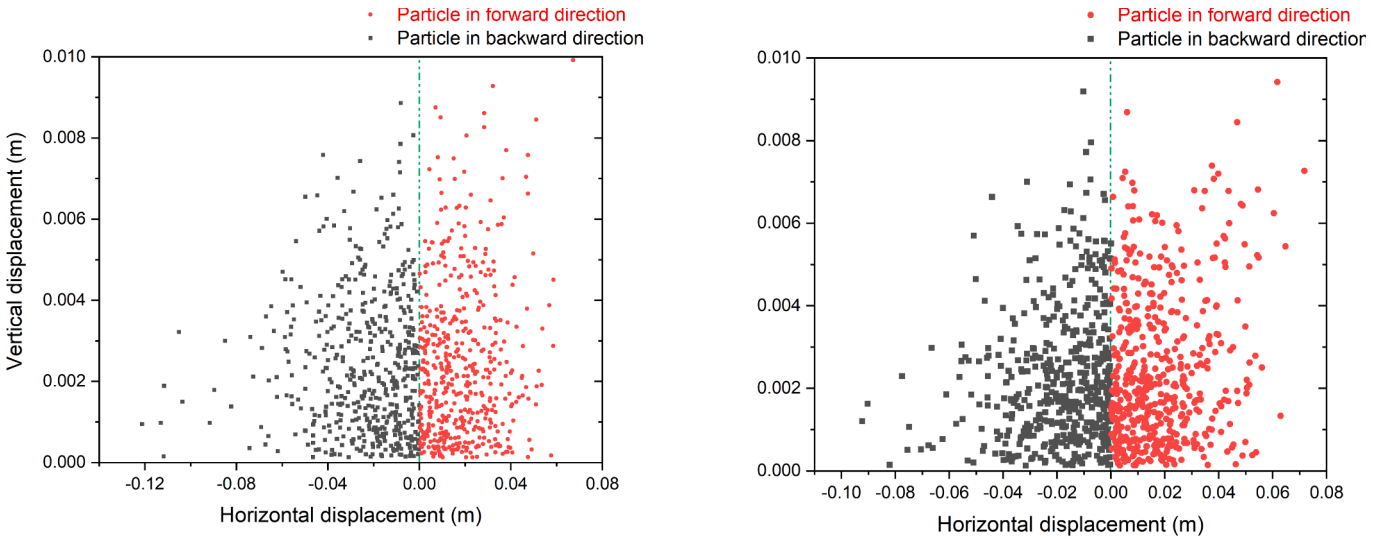


Fig. 4. Simulated results of 260 μm particle trajectory with different initial positions at 110 Hz, 'hopping mode', reproduced from [33] ("with permission").



(*a*) With DEP (b) Without DEP

Fig. 5. Scatter plot of particle positions at the frequency of 100 Hz for a particle of 250 μm with random initial position.

proportional to the square of particle size. According to formula (10), $F_{dep} \propto r^3$, so DEP is volume related. While the forces are of a similar magnitude, the DEP becomes more dominant as the particle size increases. This balance between DEP and Coulomb force is a function of particle size suggesting that separation of particles by size may be possible.

3. Direction of particle motion

3.1. Motin related to initial positions

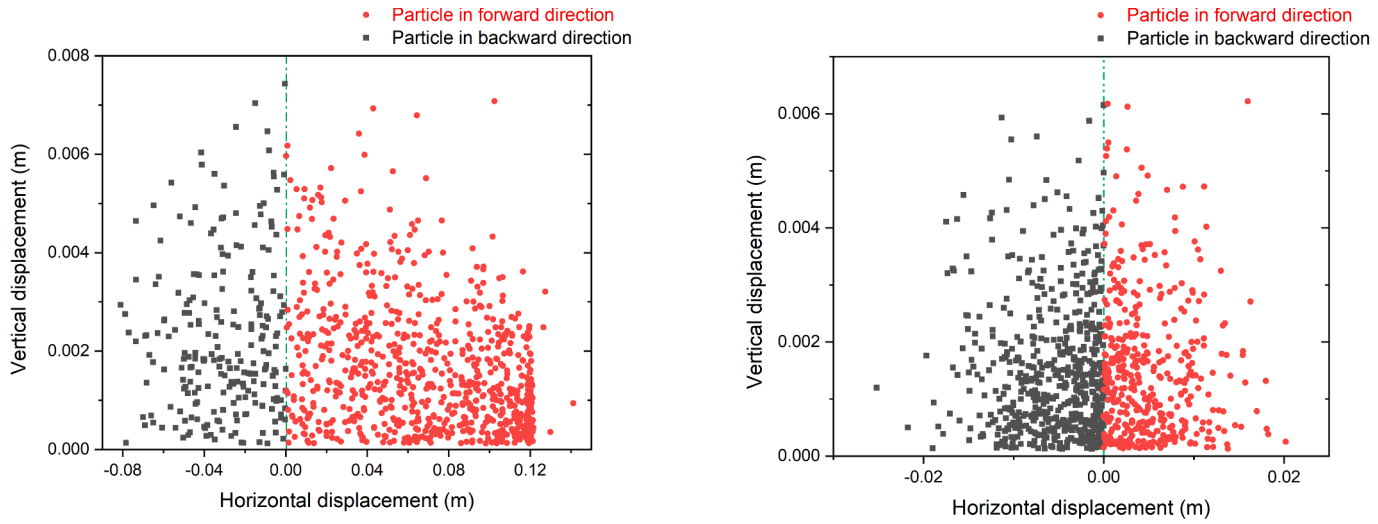
Single particle simulations qualitatively demonstrate the effect of forces and operating parameters on the particle motion. Analysis of how the operating parameters affect the motion of particles as a function of size allow prediction of the motion of multiple particles and applications involving separation by size.

As a result of particle collisions, curtain mode and surfing mode motions are difficult to maintain. We will focus therefore on hopping mode. In the theory for particle motion in ETW waves [33], we found that particle trajectories could be affected by initial position and exhibited different moving directions in the hopping mode, especially at higher frequencies, shown in Fig. 4. In the plot, x_0 means the initial position in our simulation set and λ is the wavelength.

Using the same mode as in [33], it is possible to predict the direction of travel for particles. We set the particle diameter at 250 μm and the particle charge at 5 % of the saturation charge. We ran the simulation at 100 Hz selecting 1000 random initial positions across a wavelength and recorded their relative displacements after a time of 0.5 s. We chose a time interval of 0.5 s because the experimental board is 0.2 m long, aligning with the average distance particles cover within that time frame. The relative positions are shown in Fig. 5 (*a*). The number of particles in forward direction is 489, which means the estimated probability for the particle moving forward is 48.9 %. We have done the same simulation without DEP and the result is shown in Fig. 5 (b). The particle in Fig. 5 (b) moves further away in the forward direction. The comparison of (a) and (b) shows that adding DEP increases the probability of particles moving in the forward direction. However, the effect of DEP on backward motion is less significant, and affects mainly particle motion close to surface, as DEP decays much faster than Coulomb force as particle levitate away from the surface.

3.2. Effect of frequency, particle size and charge

At low frequencies, the wave velocity is low and particles can de driven by the electrostatic traveling wave to move synchronously. The first order wave is dominant, so most of the particles will follow along



(a) 40 Hz (b) 200 Hz

Fig. 6. Scatter plot of particle positions for a particle of 250 μm with random initial position at different frequencies.

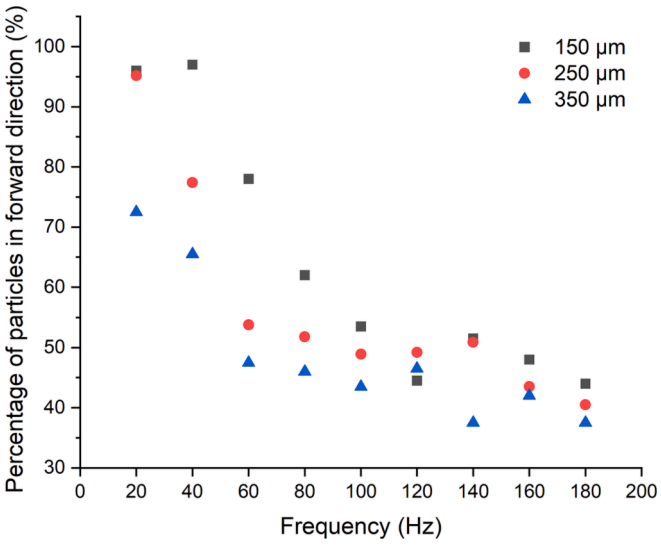


Fig. 7. Relationship between the percentage of particles in forward direction and frequency based on the simulation results.

the wave in the forward direction. Fig. 6 (a) shows the final positions of 1000 particles with a random starting position at a frequency of 40 Hz. The number of particles in the forward direction is 774.

When the frequency increases, the wave velocity increases. Due to the action of the air drag force, the particle can not keep up with the traveling wave. If the wave field travels at a high speed, the accelerated and decelerated regions intersect through the particle. The subsequent movement direction is determined by the frequency and intensity of forward and backward accelerations. The forces induced by Coulomb forces in both positive and negative directions counterbalance each other, making the effect of DEP more pronounced. Therefore, particles have a larger chance to move backward at higher frequencies. Fig. 6 (b) presents simulation results at 200 Hz, the fraction of the particles in the backward direction increases compared with at low frequencies. The traveling distance also decreases with an increase of frequency, which demonstrates the counterbalancing effects of forward and backward waves.

As the particle size increases, the saturation charge decreases [39]. We assume that the saturation rate for particle size at 150 and 350 μm are 10 % and 2 % based on the charge measurement [33]. The charge and size of the particles are the critical factors affecting particle motion. Simulations were carried out recording the fraction of particles of different size moving in the forward direction at various frequencies, as

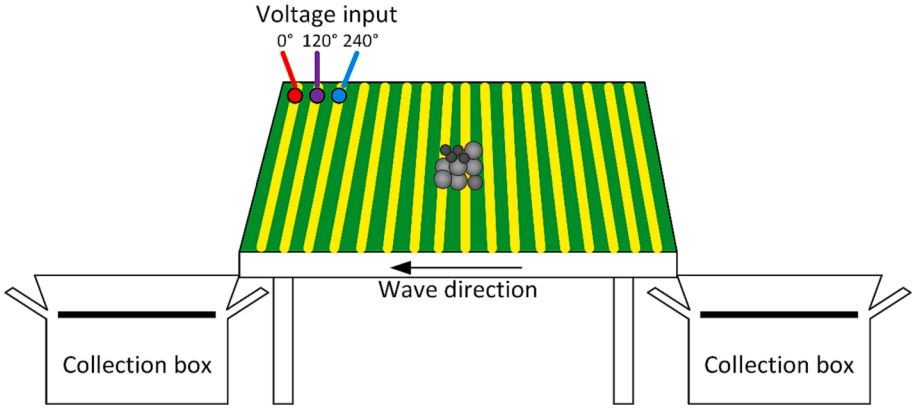


Fig. 8. Illustration of the experimental set-up.

Table 1
List of experiment parameters.

Parameters	Value	Unit
Applied voltage wave type	Sinusoidal wave	
Applied voltage wave phases	3	
Applied voltage frequency, f	20–800	Hz
Applied voltage amplitude, V_A	1500	V
Electrode width, d	1	mm
Electrode pitch, p	2	mm
ETW board length	200	mm
ETW board width	90	mm
Wavelength, λ	6	mm
Particle type	ballotini	
Particle size	30–400	μm
Particle density, ρ	2.5	kg/m^3
Particle relative permittivity, ε_m	3.7	

shown in Fig. 7. It is evident that as the frequency increases, the fraction of particles moving forward decreases. The results of Fig. 7 also demonstrate that larger particles tend to move backward at lower frequencies, while a large percentage of the smaller particles travel in the forward direction.

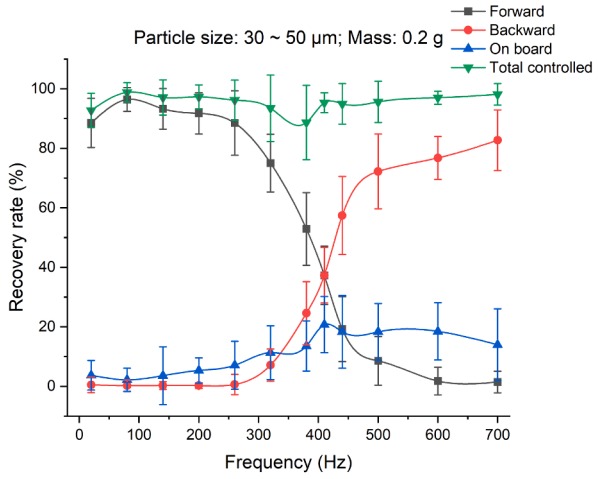
The above simulation results suggest that a system operating at a specific frequency could be used to separate particles by size.

4. Experimental validation

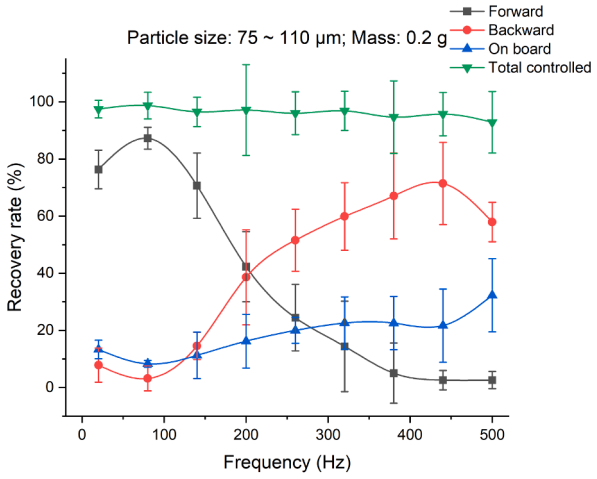
4.1. Device fabrication

The key component of the system is the conveyor board, constructed using printed circuit board (PCB) technology. The PCB comprises the top and bottom surface, featuring parallel electrodes made of copper. These electrodes on the top surface are interconnected with the connecting electrodes on the back via copper-filled holes. This allows for the division of the electrodes on the top surface into different groups, each of which can be supplied with a different voltage phases. Additionally, the board's surface is coated with a thin solder mask.

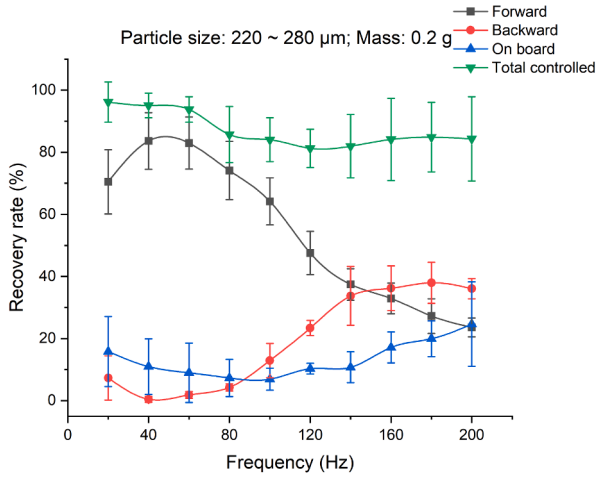
The schematic of the experimental platform is illustrated in Fig. 8. Three-phase high voltage is applied to the electrodes. The voltage is supplied by a high voltage amplifier (HAR42-4, hivolt.de) and controlled by an arbitrary waveform generator (TGA1244, TTi), both of which have four channels. The wave direction can be controlled by adjusting the phase difference. Particles introduced into the field can be transported either forward or backward.



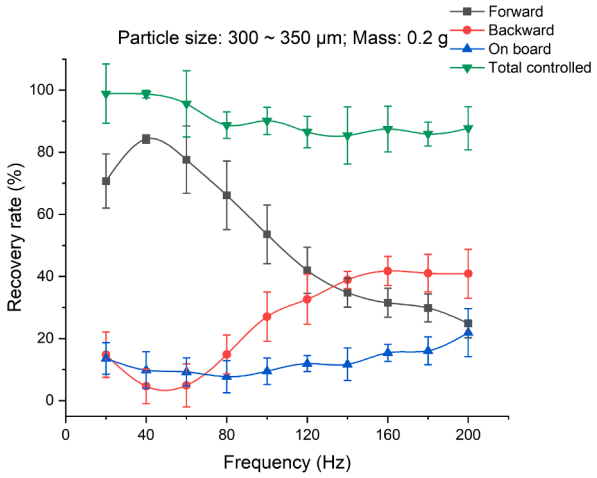
(a) Particle size at 30 ~ 50 μm



(b) Particle size at 75 ~ 110 μm



(c) Particle size at 220 ~ 280 μm



(d) Particle size at 300 ~ 350 μm

Fig. 9. Relationship between the transport (recovery with error bars) and frequency for four different size group of particles.

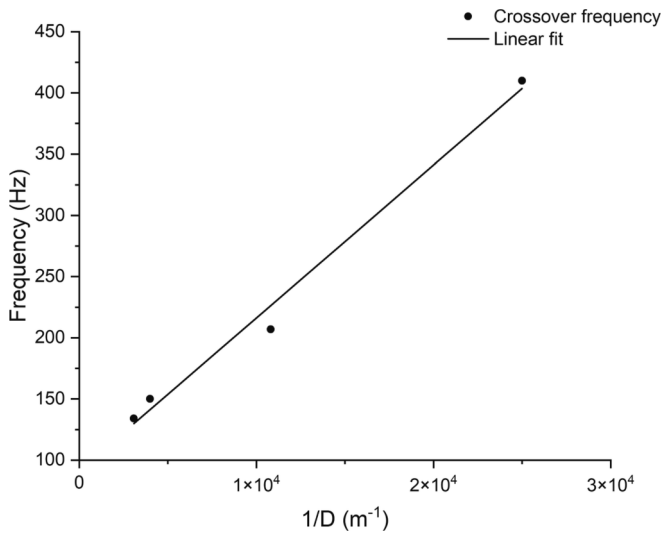


Fig. 10. Relationship between the crossover frequency and the reciprocal of particle diameter.

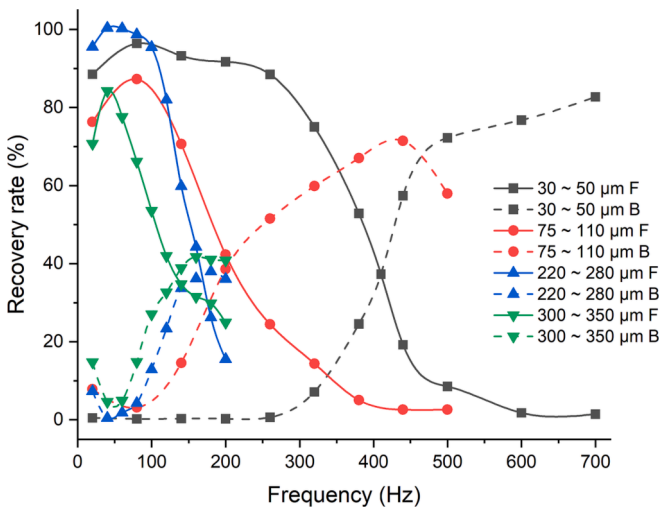


Fig. 11. Relationship between the transport (average recovery) and frequency for four different size group of particles.

4.2. Experiment parameters

In the experiments, the selection of particles and the operating parameters are provided in Table 1. The ballotini particles (glass beads) used in these experiments, are heated before the testing to reduce effects of moisture and aggregation. A three phase sinusoidal waveform is chosen because it is standard in the literature and is readily simulated. To prevent charge breakdown, the amplitude is limited to 1500 V. The electrode width and pitch are set at 1 mm and 2 mm, respectively, and these values can be adjusted through the design of the PCB structure. In our research, the primary factors under investigation are frequency and particle size.

4.3. Experiment methodology

In our protocol, we placed a measured mass (m_i) of particles in the middle of the platform. When activated, the system transports particles across the surface to be collected in the boxes on each end. The mass of the collected particles in the forward direction and backward direction are weighed and recorded as m_f and m_b. In the experiment, the mass of the particles remaining on the board is also measured and recorded as m_s. Because a few particles may fly away from the board, the sum of m_f, m_b and m_s is slightly smaller than 100 %. The forward and backward recovery rate is calculated as $R_f = m_f/m_i$ and $R_b = m_b/m_i$, respectively. The sum of m_f, m_b and m_s represents the total particles that can be controlled. Controlled particles refer to the particles that we can manipulate, either by collecting them in the forward or backward direction or keeping them on the board.

5. Results and discussion

5.1. Measurement of particle transport

Four groups of particle size were tested, 30–50 μm, 75–110 μm, 220–280 μm, and 300–350 μm. The relationship between the recovery rate and frequency is shown in following Fig. 9. The mass in the top title of the figures means the m_i. The experiments have been repeated at least 6 times at each data point and the error bars represents the 95 % confidence interval.

These data points are connected by the spline line fit using the Origin software. There is a crossover point on the forward and backward recovery rate line. The frequency corresponding this point we define as the crossover frequency. At this frequency, a particle is equally likely to move along or against the traveling wave.

From Fig. 9, it is clear that a very large percent of particles move in the forward direction at low frequencies. As the frequency increases, the fraction of particles being transported backward increases. In addition, at high frequencies, the blue line shows that the amount of particles staying on the board increases, indicating that the ability of the electrostatic traveling wave to transport particles decreases.

The scatter plot of the relationship between the crossover frequency and the inverse of particle size is shown in Fig. 10. The crossover frequency decreases as the particle size increases. A linear regression line is used to model the relationship. The expression is:

$$f = \frac{0.125}{D} + 91.4 \tag{11}$$

where D is the diameter of the particle. The Pearson correlation coefficient is 0.995.

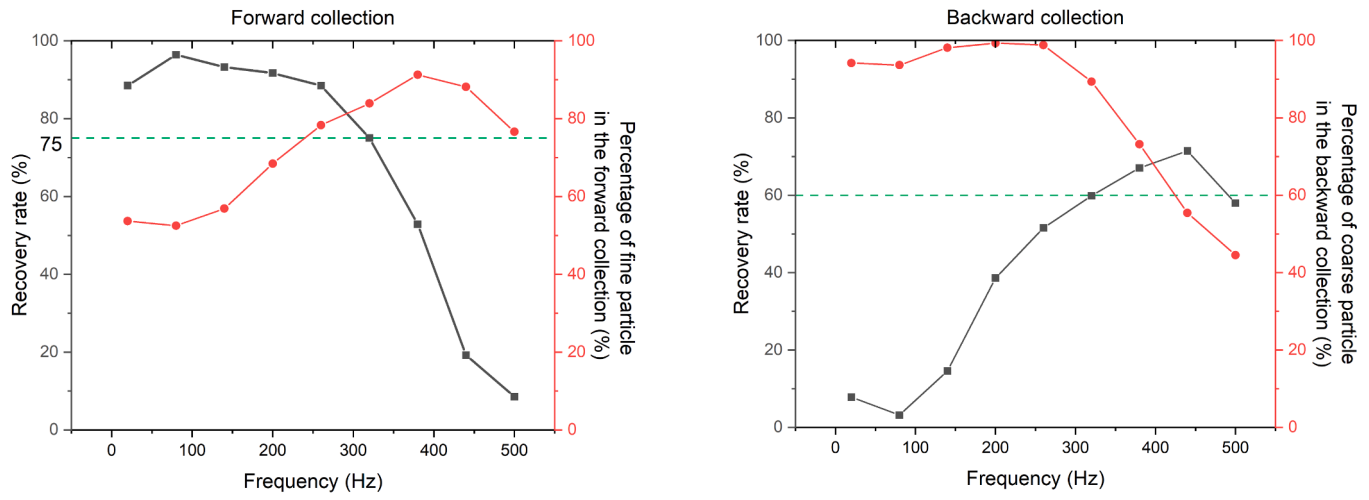
The forward and backward recovery rate lines of four groups of sizes in the plots of Fig. 9 are combined in Fig. 11. It is evident that the proportion of forward and backward motion for particles of different sizes may exhibit significant differences at the same frequencies. This research suggest that it is possible to separate particles with different sizes in terms of direction of transport by selecting appropriate frequencies.

5.2. Prediction of particle size separation

If we assume that a mixture of particles will behave in a manner very similar to that as predicted and measured with single particles then the forward and backward collection rates can be predicted. Consequently, size sorting performance can be predicted.

The particles of larger size tend to move backward at lower frequencies, at which frequency the small particles may still move forward effectively. Therefore, transporting the mixture at appropriate frequencies cause small particles to concentrate in the collection box in the forward direction, and larger particles to concentrate in the backward collection. Fig. 12 shows the prediction of the separation performance for the mixture of size groups of 30–50 μm and 75–110 μm with equal initial mass as a function of frequency. The data points are calculated by the mean data points of the single size class transport runs. Fig. 12 (a) depicts the relationship between the recovery rate and concentration of fine particles (30–50 μm) with the operating frequency in the forward collection. Meanwhile Fig. 13 12 (b) pertains to the coarse particles (75–110 μm).

In the size sorting process, both the recovery rate and concentration



(a) Fine particle in the forward collection

(b) Coarse particle in the backward collection

Fig. 12. Estimation of particle separation performance at different frequencies from single size transport experiment.

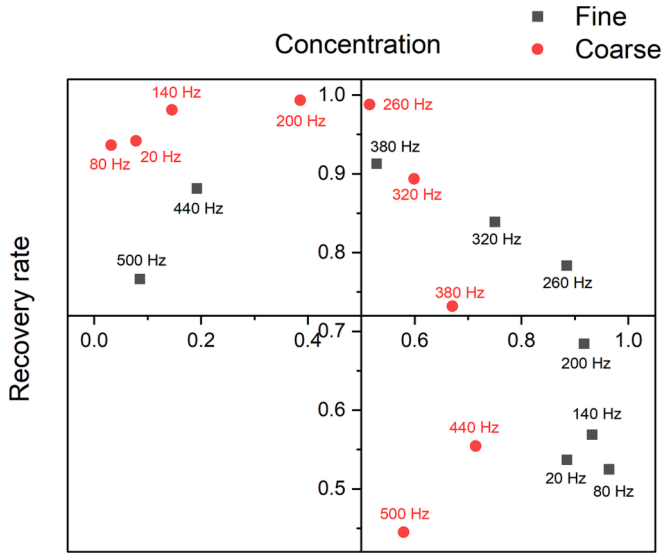


Fig. 13. Relationship between the separation results of the recovery rate and concentration of particles with the frequency.

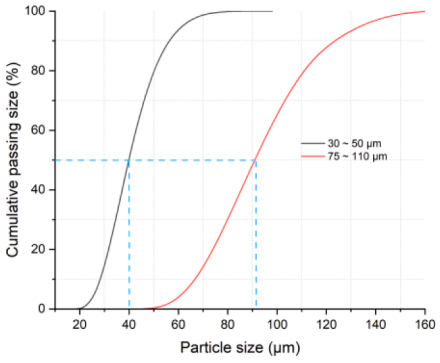


Fig. 14. Size distribution of the original sample.

of fine particles reach level higher than 75 % when conducting the experiment within the frequency range from 240 Hz to 320 Hz. In the backward collection, the concentration of coarse particles remains very high, larger than 90 %, at the frequency from 20 Hz to 320 Hz. This is because that the small particles move very effectively forward at low frequencies and only coarse particles move backward. The recovery rate of coarse particles in the backward collection is also minimal at low frequencies. As the frequency increases, the recovery rate of coarse particles increases. In the frequency range of 320–425 Hz, the recovery rate and concentration for coarse particles in the backward collection can be larger than 60 %.

Based on the same dataset, the scatter centre plot is shown in Fig. 13. The region in the top right quadrant has both high recovery rate and concentration for fine and coarse particles. From this chart we can evaluate the appropriate frequencies for the given mixture.

5.3. *Particle separation experimental results*

In the separation experiments, we selected two groups of particles: 30–50 μm and 75–110 μm. The mass of each group was 0.5 g. The size distribution of the two groups of particles were measured by the Mastersizer, which is shown in Fig. 14. In each experiment, 0.5 g of each group were mixed and fed into the board. The mass of the particles collected in the forward and backward bins were measured and the size distribution of each collection were analysed by the Mastersizer.

Based on the estimation of separation performance of Fig. 14 in section 5.2, the operating frequency from 260 to 380 Hz works well for both fine and coarse particles. The operating frequency was tested at 350 Hz. The size distribution in the forward and backward collection were compared in Fig. 15. Backward collection is the same as coarse particle size distribution. Forward collection size distribution tends toward fine but is coarser than the initial fine sample particle size distribution.

We also used a 50 μm sieve to separate particles in the forward and backward collection and measured the mass of the fine and coarse particles, seen as Fig. 16. These results also show the good separation performance.

The separation processes were also tested at of 250 Hz and 450 Hz. The results are shown in Fig. 17 and Fig. 18. At the lower frequency, forward collection is coarser than at 350 Hz suggesting more coarse particles move forward. At high frequency, more fines in coarse stream. This was because at lower frequencies, particles were more likely to

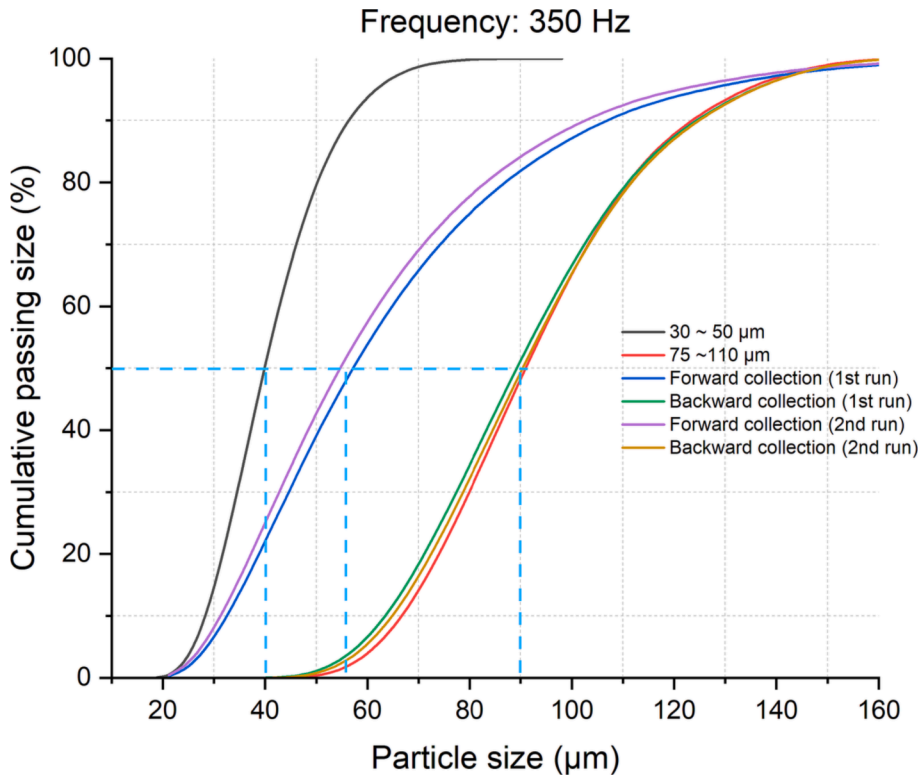


Fig. 15. Particle separation results at 350 Hz.

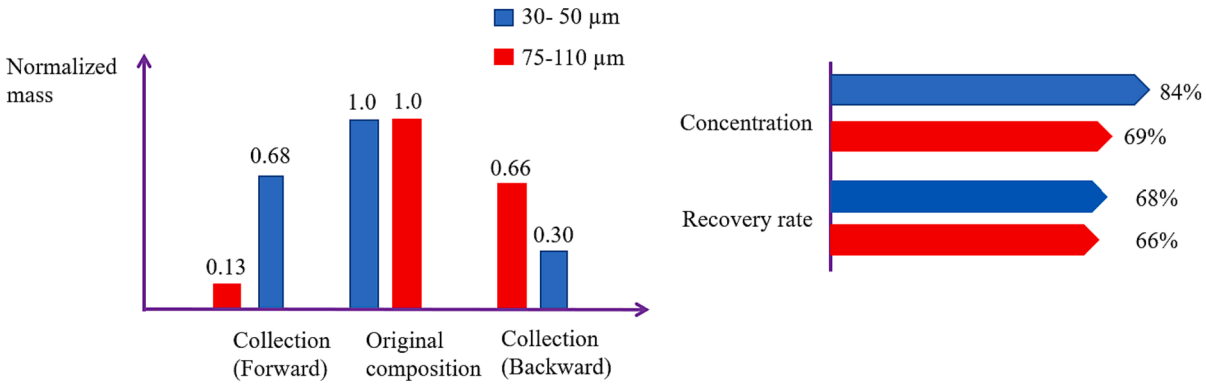


Fig. 16. Mass distribution of different sizes of particle in the forward and backward collection.

move forward, especially for the smaller sizes. In this way, small size particles rarely moved backward, and the backward box could collect nearly pure big particles. However, in the forward direction, more larger particles may also be collected at lower frequency, so the separation for small size particles in the forward direction was poor. Likewise, at higher frequencies, the forward collection could enhance recovery for smaller sizes, while the backward collection showed reduced recovery for larger sizes.

In each experiment, the total mass of the particles in the forward collection and backward collection were also measured, which was plotted in Fig. 19 with error bars. In addition, the estimation of the mass recovery using the single particle transport results is shown in the red line for comparison. They have good agreement. This confirms that mixing particles with relatively large size difference does not significantly affect the inherent directional characteristics of particle motion. The transport results of four groups of particle sizes can serve as a guide for selecting the separation frequency.

6. Conclusions

Theoretical analyses and simulations have been investigated for the separation of particles using ETW system. Based on the frequency effect on particle motion direction, the separation for ballotini with different sizes have been tested and shown good performance. The main findings are described below.

1. Our simulation analysis have shown that both the first harmonic wave Coulomb and DEP forces contribute the backward motion of the particles. The particle has a higher probability to move backward at higher frequencies.
2. We have found and defined a crossover frequency, at which a particle is equally likely to move along or against the traveling wave. This critical frequency decreases as the particle size increases. We can use this parameter as a baseline to adjust upward or downward to select the appropriate frequencies to separate particles by size.

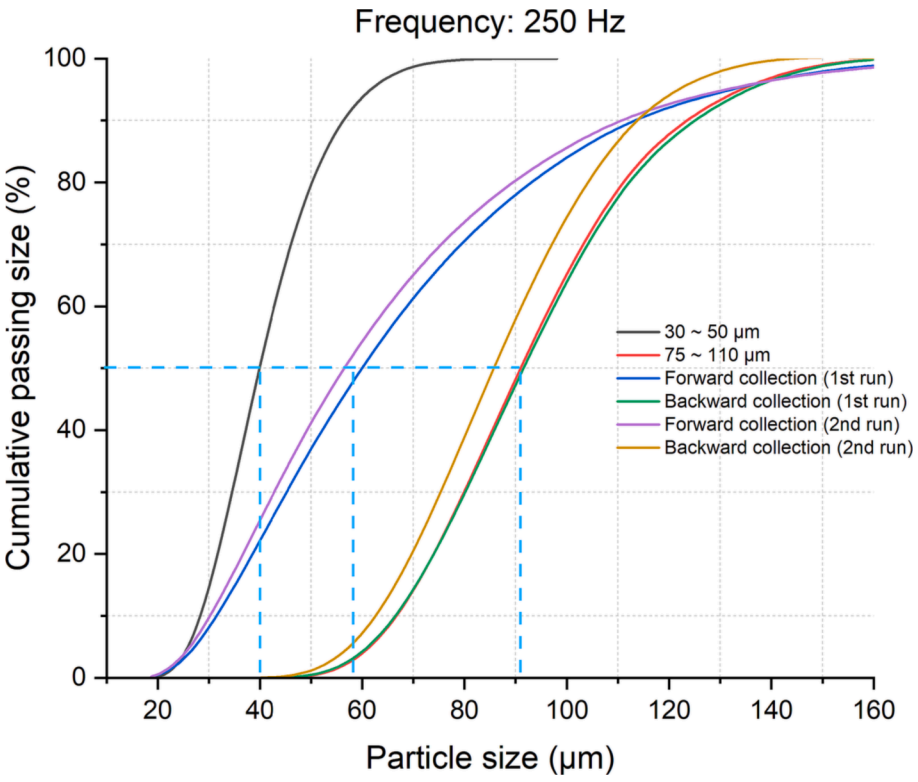


Fig. 17. Particle separation results at 250 Hz.

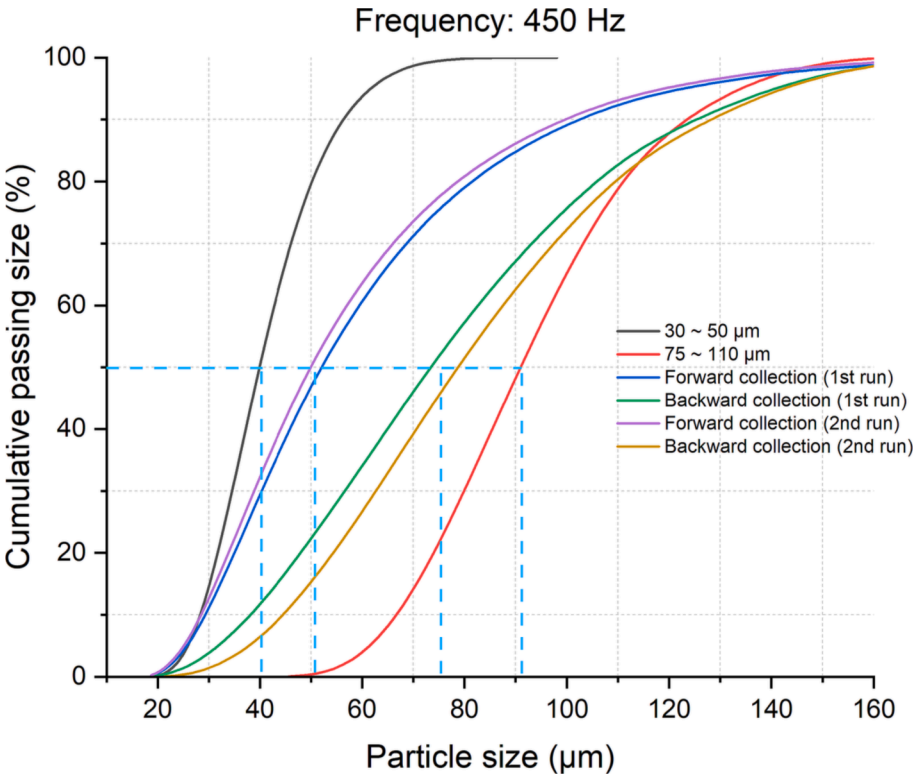


Fig. 18. Particle separation results at 450 Hz.

3. We have demonstrated experimentally the successful separation of particles with different sizes, which are between 30–50 μm and 75–110 μm. The concentration of the collected desired particle can be over 90 % and the recovery rate can exceed 79 %.

CRediT authorship contribution statement

Yue Yu: Conceptualization, Formal analysis, Investigation, Methodology, Software, Validation, Visualization, Writing – original draft.

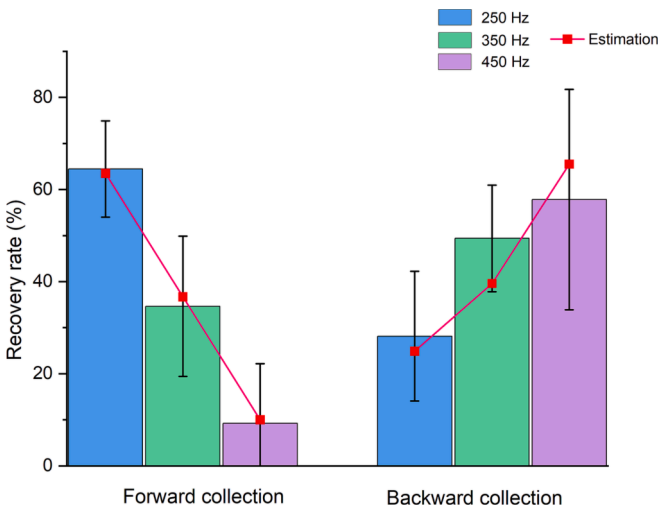


Fig. 19. Mass measurements for the forward and backward collection at the different frequencies and a comparison with single particle estimates.

Jan Cilliers: Conceptualization, Methodology, Resources, Writing – review & editing, Supervision. **Kathryn Hadler:** Conceptualization, Formal analysis, Methodology, Supervision, Writing – review & editing. **Stanley Starr:** Conceptualization, Investigation, Methodology, Supervision, Writing – review & editing. **Yanghua Wang:** Conceptualization, Project administration, Supervision.

Declaration of competing interest

The authors declare that they have no known competing financial interests or personal relationships that could have appeared to influence the work reported in this paper.

Data availability

No data was used for the research described in the article.

Acknowledgment

The authors are grateful to the sponsors of Resource Geophysics Academy, Imperial College London, for supporting this research.

References

[1] T. Hirajima, H.T.B.M. Petrus, Y. Oosako, M. Nonaka, K. Sasaki, T. Ando, Recovery of cenospheres from coal fly ash using a dry separation process: Separation estimation and potential application, Int. J. Miner. Process. 95 (2010) 18–24.
[2] P.J. Borm, Toxicity and occupational health hazards of coal fly ash (CFA). A review of data and comparison to coal mine dust, The Annals of occupational hygiene, 41 (1997) 659-676.
[3] J. Oshitani, G.V. Franks, M. Griffin, Dry dense medium separation of iron ore using a gas–solid fluidized bed, Adv. Powder Technol. 21 (2010) 573–577.
[4] S.K. Tripathy, P.K. Banerjee, N. Suresh, Y.R. Murthy, V. Singh, Dry High-Intensity Magnetic Separation In Mineral Industry—A Review Of Present Status And Future Prospects, Miner. Process. Extr. Metall. Rev. 38 (2017) 339–365.
[5] J.N. Rasera, J.J. Cilliers, J.A. Lamamy, K. Hadler, The beneficiation of lunar regolith for space resource utilisation: A review, Planet. Space Sci. 186 (2020) 104879.
[6] H. Yano, T. Kubota, H. Miyamoto, T. Okada, D. Scheeres, Y. Takagi, K. Yoshida, M. Abe, S. Abe, O. Barnouin-Jha, Touchdown of the Hayabusa spacecraft at the Muses Sea on Itokawa, Science 312 (2006) 1350–1353.
[7] H. Kawamoto, K. Tsuji, Manipulation of small particles utilizing electrostatic force, Adv. Powder Technol. 22 (2011) 602–607.
[8] Y. Yu, J. Cilliers, K. Hadler, S. Starr, Y. Wang, A review of particle transport and separation by electrostatic traveling wave methods, J. Electrostat. 119 (2022) 103735.
[9] S. Masuda, K. Fujibayashi, K. Ishida, H. Inaba, Confinement and transportation of charged aerosol clouds via electric curtain, Electr. Eng. Jpn. 92 (1972) 9–18.
[10] S. Masuda, T. Kamimura, Approximate methods for calculating a non-uniform travelling, J. Electrostat. 1 (1975) 351–370.
[11] S. Masuda, Y. Matsumoto, Theoretical Characteristics of Standing-Wave Electric Curtains, Electr. Eng. Jpn. 93 (1973) 41–54.
[12] S. Masuda, M. Washizu, M. Iwadare, Separation of Small Particles Suspended in Liquid by Nonuniform Traveling Field, IEEE Trans. Ind. Appl. 23 (1987) 474–480.
[13] S. Masuda, M. Washizu, I. Kawabata, Movement of Blood Cells in Liquid by Nonuniform Traveling field, IEEE Trans. Ind. Appl. 24 (1988) 217–222.
[14] A.C. Yen, C.D. Hendricks, A planar electric curtain used as a device for the control and removal of particulate materials, J. Electrostat. 4 (1978) 255–267.
[15] F.W. Schmidlin, A new nonlevitated mode of traveling wave toner transport, IEEE Trans. Ind. Appl. 27 (1988) 480–488.
[16] F.W. Schmidlin, Modes of traveling wave particles transport and their applications, J. Electrostat. 34 (1995) 225–245.
[17] W. Machowski, W. Balachandran, D. Hu, Influence of electrode geometry on transport and separation efficiency of powders using traveling wave field technique, in: IEEE Industry Applications Conference Thirtieth IAS Annual Meeting, 1995.
[18] J. Gu, X. Qian, Y. Liu, Q. Wang, Y. Zhang, X. Ruan, X. Deng, Y. Lu, J. Song, H. Zhang, Y. Dong, M. Wei, S. Li, W.H. Wang, Z. Zou, M. Yang, W. Yao, (2023).
[19] J.K.W. Chesnutt, J.S. Marshall, Simulation of Particle Separation on an Inclined Electric Curtain, IEEE Trans. Ind. Appl. 49 (2013) 1104–1112.
[20] G.Q. Liu, J.S. Marshall, Effect of particle adhesion and interactions on motion by traveling waves on an electric curtain, J. Electrostat. 68 (2010) 179–189.
[21] M. Adachi, H. Moroka, H. Kawamoto, S. Wakabayashi, T. Hoshino, Particle-size sorting system of lunar regolith using electrostatic traveling wave, J. Electrostat. 89 (2017) 69–76.
[22] A. Zouaghi, N. Zouzou, Impact of spatial harmonic waves on dielectric particles displacement in standing and traveling wave electric fields, J. Electrostat. 98 (2019) 25–33.
[23] A. Zouaghi, N. Zouzou, Numerical modeling of particle motion in traveling wave solar panels cleaning device, J. Electrostat. 110 (2021) 103552.
[24] A. Zouaghi, N. Zouzou, P. Braud, Study of dielectric particles motion in traveling and standing electrostatic waves using particle tracking velocimetry, J. Phys. D Appl. Phys. 53 (2020) 385502.
[25] A. Zouaghi, N. Zouzou, L. Dascalescu, Assessment of forces acting on fine particles on a traveling-wave electric field conveyor: Application to powder manipulation, Powder Technol. 343 (2019) 375–382.
[26] M. Mazumder, C. Elinger, K. O'Connor, R. Eriksen, A. Bernard, M.N. Horenstein, J. Yellowhair, N. Joglekar, S. Garner, J. Bones, C. Morales, H. Acuña, Industrial Production and Field Evaluation of Transparent Electrodynamic Screen (EDS) Film for Water-Free Cleaning of Solar Collectors, in: IEEE (Ed.) 2019 IEEE 46th Photovoltaic Specialists Conference (PVSC), IEEE, 2019, pp. 3269-3276.
[27] M. Mazumder, M.N. Horenstein, N.R. Joglekar, A. Sayyah, J.W. Stark, A.A. R. Bernard, S.M. Garner, J.E. Yellowhair, H.Y. Lin, R.S. Eriksen, A.C. Griffin, Y. Gao, R.L. Centra, A.H. Lloyd, Mitigation of Dust Impact on Solar Collectors by Water-Free Cleaning With Transparent Electrodynamic Films: Progress and Challenges, IEEE J. Photovoltaics 7 (2017) 1342–1353.
[28] A. Sayyah, R.S. Eriksen, M.N. Horenstein, M.K. Mazumder, Performance Analysis of Electrodynamic Screens Based on Residual Particle Size Distribution, IEEE J. Photovoltaics 7 (2017) 221–229.
[29] J. Gu, G. Zhang, Q. Wang, C. Wang, Y. Liu, W. Yao, J. Lyu, Experimental study on particles directed transport by an alternating travelling-wave electrostatic field, Powder Technol. 397 (2022) 117107.
[30] S.J. Williams, J.D. Schneider, B.C. King, N.G. Green, Particle-Induced Electrostatic Repulsion within an Electric Curtain Operating below the Paschen Limit, Micromachines (basel) 13 (2022) 288.
[31] B. Guo, W. Javed, Y.S. Khoo, B. Figgis, Solar PV soiling mitigation by electrodynamic dust shield in field conditions, Sol. Energy 188 (2019) 271–277.
[32] C.I. Calle, C.R. Buhler, M.R. Johansen, M.D. Hogue, S.J. Snyder, Active dust control and mitigation technology for lunar and Martian exploration, Acta Astronaut. 69 (2011) 1082–1088.
[33] Y. Yu, J. Cilliers, K. Hadler, S. Starr, Y. Wang, The motion of small particles in electrostatic travelling waves for transport and separation, Powder Technol. 425 (2023).
[34] J.R. Melcher, E.P. Warren, R.H. Kotwal, Theory for Pure-Traveling-Wave Boundary-Guided Transport of Tribo-Electrified Particles, Part. Sci. Technol. 7 (1989) 1–21.
[35] J.R. Melcher, E.P. Warren, R.H. Kotwal, Theory for Finite-Phase Traveling-Wave Boundary-Guided Transport of Triboelectrified Particles, IEEE Trans. Ind. Appl. 24 (1989) 949–955.
[36] H.A. Pohl, The motion and precipitation of suspensoids in divergent electric fields, J. Appl. Phys. 22 (1951) 869–871.
[37] X.-B. Wang, Y. Huang, F. Becker, P. Gascoyne, A unified theory of dielectrophoresis and travelling wave dielectrophoresis, J. Phys. D Appl. Phys. 27 (1994) 1571.
[38] M. Pauthenier, M. Moreau-Hanot, La charge des particules sphériques dans un champ ionisé, J. Phys. Radium 3 (1932) 590–613.
[39] R.D. Cruise, K. Hadler, S.O. Starr, J.J. Cilliers, The effect of particle size and relative humidity on triboelectric charge saturation, J. Phys. D Appl. Phys. 55 (2022).